Nanoscale

Accepted Manuscript

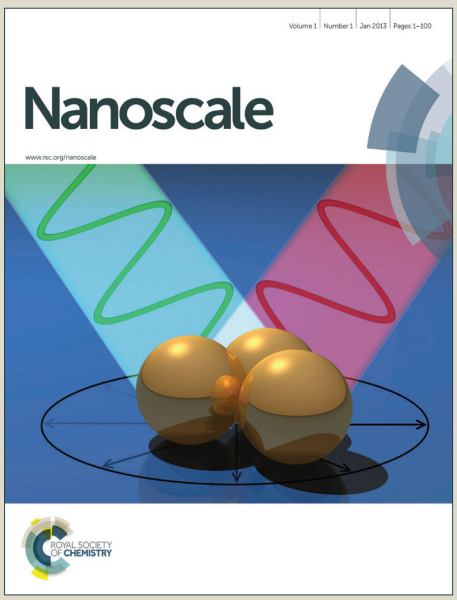

ROYAL SOCIETY OF CHEMISTRY

www.rsc.org/nanoscale

Nanoscale

Article

Thermal Conductivity from Hierarchical Heat Sinks Using Carbon Nanotubes and Graphene Nanosheets

Received 00th January 20xx,
Accepted 00th January 20xx

DOI: 10.1039/x0xx00000x

www.rsc.org/

Chien-Te Hsieh,*[a] Cheng-En Lee,[a] Yu-Fu Chen,[a] Jeng-Kuei Chang,[b] and Hsi-sheng Teng*[c]

The in-plane (k_{ip}) and through-plane (k_{tp}) thermal conductivities of heat sinks using carbon nanotubes (CNTs), graphene nanosheets (GNs), and CNT/GN composite are extracted from two experimental setups within the 323–373 K temperature range. Hierarchical three-dimensional CNT/GN framework displays the higher k_{ip} and k_{tp} values, as compared to the CNT- and GN-based heat sinks. The k_{ip} and k_{tp} values of CNT/GN-based heat sink reach as high as 1991 and 76 W/m K at 323 K, respectively. This improved thermal conductivity is attributed to the fact the hierarchical heat sink offers a stereo thermal conductive network that combines point, line, and plane contact, leading to better heat transport. Furthermore, the compression treatment provided an efficient route to increase both k_{ip} and k_{tp} values. This result reveals that the hierarchical carbon structures become denser, inducing more thermal conductive area and less thermal resistivity, i.e., a reduced possibility of phonon-boundary scattering. The correlation between thermal and electrical conductivity (ε) can be well described by two empirical equations: k_{ip} = 567 ln (ε) + 1120 and k_{tp} = 20.6 ln (ε) + 36.1. The experimental results are obtained within the temperature range of 323-373 K, suitably complementing the thermal management of chips for consumer electronics.

Introduction

Both carbon nanotubes (CNTs) and graphene nanosheets (GNs) have sparked promising scientific and technological interests due to their exceptional electrical and thermal properties, showing great potential in a variety of applications.[1] With the ever decreasing size of electronic and nano-mechanical devices, there is an increasing demand in the nano-structural carbon materials (e.g., CNTs and GNs) that conduct heat efficiently, thus, preventing thermal damage to electronic components.[2] Recently, a number of pioneering researches have been devoted to applying them in integrated circuits and thermal management. In fact, the discovery of CNTs in 1991 has imparted the speculation that the one-dimensional carbon could possess a thermal conductivity equal to or higher than that of diamond and graphite.[3,4] The other carbon material, GN, consists of one or few layers of atoms arranged in a honeycomb lattice,[5,6] exhibiting thermal conductivity of 4840–5300 W/m K for a single-layer graphene.[7,8] Although, both CNTs and GNs possess high theoretical thermal conductivities, an ideal strategy for preparing high-performance heat sink, based on the nano-structural carbon materials, to resolve thermal management problems is still challenging.[9]

It is generally recognized that natural crystalline graphite shows a thermal conductivity of 2200 W/m K in its (002) crystal plane, whereas commonly poly-crystalline graphite reaches only as low as 70–150 W/m K at ambient temperature.[10] Previous study has pointed out that the basal-plane thermal conductivity can be obviously enhanced by tuning the orientation of graphite platelets.[11] For instance, a thermal treatment incorporated with hot pressing technique has been confirmed to improve the thermal conductivity of graphite composites,[12,13] resulting from a preferred orientation of crystalline graphite lamellae. The experimental results reveal two crucial points: (i) thermal transport in *a*-axis of graphite lattice is much higher than that in *c*-axis (i.e., in-plane thermal conductivity (k_{ip}) > through-plane thermal conductivity (k_{tp}), and (ii) thermal conductivity of graphite strongly depends on phonon transport along the basal plane (i.e., the mean free path of phonon is related to average crystallite size). This reflects that thermal transport capability of graphite-based materials is strongly influenced by structural factors such as defects, edges, broken bonds and voids.[14,15] As the extent of resistive thermal junctions increases, the thermal conductivity drops. This finding directs us toward exploring the thermal properties of CNT-, GN-, and CNT/GN-based heat sinks. To date, few work have reported in-plane and through-plane thermal conductivities from such carbon hybrids using one- and two-dimensional carbons for thermal management systems.[16]

Within the above scope, this study aims at investigating thermal conductivities from CNT, GN, and CNT/GN hybrid heat

[a]*Department of Chemical Engineering and Material Science, Yuan Ze University, Taoyuan 32003, Taiwan. E-mail: cthsieh@saturn.yzu.edu.tw; Tel: +886-3-4638800 ext.2577; Fax: +886-3-4559373.*
[b]*Institute of Materials Science and Engineering, National Central University, Taoyuan 32001, Taiwan*
[c]*Center for Micro/Nano Science and Technology, National Cheng Kung University, Tainan 70101, Taiwan. E-mail address: hteng@mail.ncku.edu.tw.*

sinks within temperature range of 323–373 K. The CNT and GN samples used here were prepared by catalytic chemical vapor deposition and modified Hummers' method,[17,18] respectively. In order to reduce thermal junction in the carbon nanostructures, a compression process was adopted to minimize void fraction of the heat sinks. The compact heat sinks, thus, induce fewer thermal interfaces and relatively high effective thermal conductivities. The present work also shed some lights on (i) how the dimension of nano-structural carbons affects the thermal conductivity of heat sinks and (ii) the relationship between electrical conductivity and thermal conductivity of heat sinks. On the basis of the experimental results, the CNT/GN heat sink offers superior thermal releasing ability with high thermal conductivity, as compared with CNT- and GN-based ones.

Experimental

Preparation of heat sinks

This work used a modified Hummers' method in preparing GN powders, which differs from the original Hummers' method in oxidizing agent concentration, oxidation period, and ratio of graphite precursor to oxidation agent.[19] The GO sheets were placed in a horizontal furnace and heated to 400°C in H_2-containing atmosphere (H_2/Ar: 5/95 in v/v). The thermal reduction was performed for 1 hr, ensuring the reduction of GO sheets and giving the GNs. The CNTs were grown by using catalytic chemical vapor deposition, in which the nickel oxide and ethylene served as metallic catalyst and carbon precursor, respectively.[17] The GN suspension was well mixed with the CNT powders in isopropanol at ambient temperature. Herein the weight ratio of CNT to GN was set at 50:50. Afterward, the mixture was placed in a high-performance homogenizer (IKA, Model T25, Germany), equipped with a rotor-stator generator. The rotor acted as a centrifugal pump to re-circulate the liquid and suspended solids through the generator, where shear, impact, collision, and cavitation provide rapid homogenization. The homogenizing dispersion process was performed with a rotation speed of 24,000 rpm for 15 min, ensuring the formation of homogeneous CNT/GN hybrid.

Three carbon materials (i.e., CNT, GN, and CNT/GN) were well mixed with a binder (poly-vinylidenefluoride, PVDF) with the weight ratio of 80:20 in solvent (N-methyl pyrrolidinone, NMP) to form the carbon slurry. For uniformity, the slurries were then blended with a three-dimensional mixer using zirconia balls for 3 min. The resultant slurries were pasted on Cu foil substrates (thickness: ~10 μm) with a doctor blade, followed by evaporating the solvent, NMP, with a blow dryer. The as-prepared heat sinks were dried at 80°C in a vacuum oven overnight and pressed under a pressure of approximately 200 kg cm^{-2}. The compressive ratio of as-prepared sheets was set at approximately 40%. The heat sinks with the compression treatment were designated to CNT', GN', and CNT/GN'.

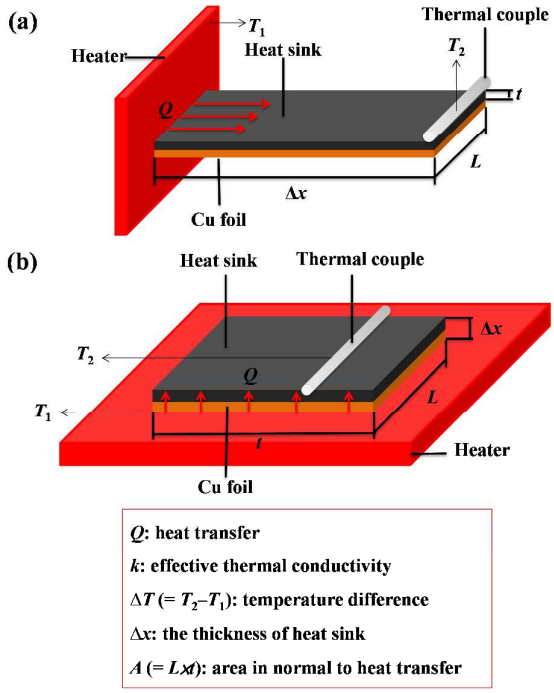

Figure 1. The schematic diagrams of experimental setup for analyzing (a) in-plane and (b) through-plane thermal conductivities of carbon-based heat sinks, using Fourier's law.

Material characterization of carbons

Field-emission scanning electron microscopy (FE-SEM; JEOL JSM-5600) was adopted to inspect the top- and cross-sectional views of heat sinks. The micro-structural observation of carbon samples was investigated by using transmission electron microscope (TEM; JEOL, JEM-2100). An X-ray diffraction (XRD; Shimadzu Labx XRD-6000) spectroscope, equipped with Cu-Kα radiation emitter, was used to characterize the crystalline structures of carbon materials. The crystalline structure of carbon samples was analyzed by Raman spectroscopy (Renishaw Micro-Raman spectrometer).

Thermal and electrical characterization of heat sinks

Thermal characterization involved measurement of k_{ip} and k_{tp} values of heat sinks. The schematic diagrams for analyzing both values are illustrated in Figure 1a,b. In the apparatus, the heat sinks were carefully insulated by heat-preservation cotton to prevent the heat transfer loss from radiative and convection transport. The apparatus accurately reproduced the temperature-dependent thermal conductivity of different standards, i.e., Cu and Al foils. Herein highly pure (i.e., 99.95%) Cu foils with an area of 20 × 50 mm served as a typical reference for calibrating the heat transfer from an electrical resistance heater. The thermal conductivity of Cu foil as a decreasing function of operating temperature was confirmed for our system. The thermal conductivity of Cu foils ranged from 388 to 379 W/m K within the temperature region of 298–373 K. Prior to any thermal analysis, a thermal imager was

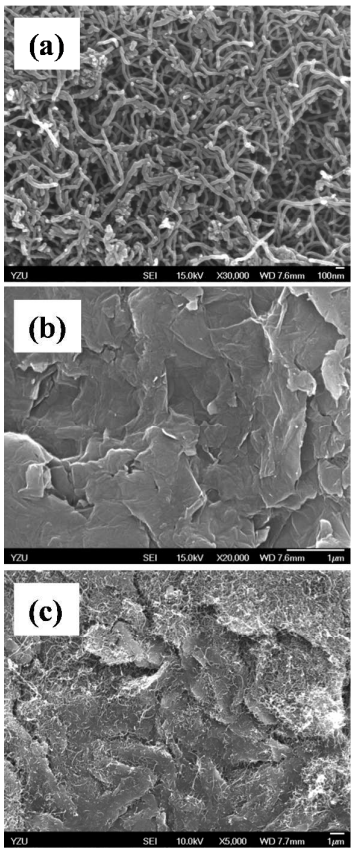

Figure 2. Top-view FE-SEM photographs of (a) CNTs, (b) GNs, and (c) CNT/GN composite.

used to observe the temperature distribution of heater. Temperature data was recorded by using five thermal couples: one on the heater, three on the heat sink, and one for measuring the ambient temperature. Each heat sink was also cut into an area of 20 × 50 mm. The effective thermal conductivity (k) of heat sink was calculated by using the Fourier's law, $Q/A = k\,\Delta T/\Delta x$, based on one-dimensional heat conduction.[20] Here Q is the amount of heat transferred through the heat sink, A is the area in normal to heat transfer direction, and ΔT is the temperature difference over the thickness of heat sink (Δx), i.e., ΔT/Δx: temperature gradient. Both k_{ip} and k_{tp} values could be obtained by comparing the temperature drops across the heat sink in the two configurations, as shown in Figure 1a,b. A four-probe resistance was measured in order to figure out the relationship between the thermal and electrical conductance. Without the regard for the geometry of heat sink, the thermal contact location on the heat sink was the same contact point of electrical resistance measurement.

Results and discussion

Figure 2a-c show top-view FE-SEM images of CNT, GN, and CNT/GN samples, respectively. As illustrated, the CNTs possess a uniform distribution in tube diameters from 30 to 60 nm and

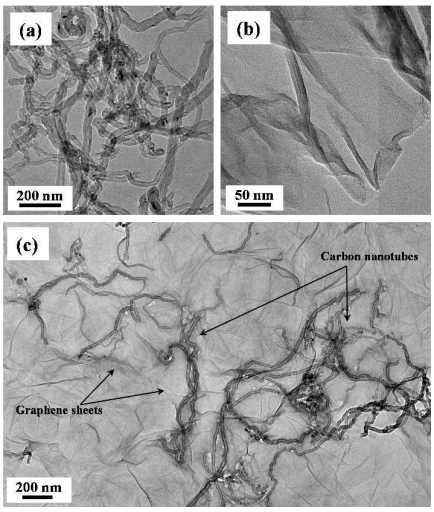

Figure 3. TEM micrographs of (a) CNTs, (b) GNs, and (c) CNT/GN composite.

an average length of several micrometers. The GO sample consists of voids, cavities, and curved layers, forming a fluffy agglomeration. This proves that the modified Hummers' method is capable of generating two-dimensional GNs obtained from the chemical exfoliation of natural graphite precursor. As for the CNT/GN hybrid, a large amount of CNTs are intercalated into the GNs after the homogenizing dispersion process. The CNT/GN hybrid creates a three-dimensional carbon framework, composed of one- and two-dimensional conductive materials. TEM was adopted to inspect the micro-structural observation of CNT, GN, and CNT/GN samples, as depicted in Figure 3a–c. These micrographs clearly illustrate that the as-grown CNTs are tubular in form, whereas the as-prepared GNs own layered structure. The GNs seem like multi-layers with an area of few micrometers. As expected, the insertion of coiled CNTs into the layered GNs enables the formation of stereo carbon network (see Figure 3c) through the homogenizing dispersion method, which has been reported previously.[21]

Figure 4 depict typical XRD patterns of different carbon samples, revealing the presence of graphite-like crystals. The diffraction peak at *ca*. $2\vartheta = 26.3°$ for the CNT sample can be assigned to the (002) peak of graphite structure, while both the (002) peaks for both the GN and CNT/GN samples shift to more negative position. Based on the calculation of Bragg's equation, the interlayer distance (d_{002}) of CNT sample is approximately 0.338 nm, close to the highly oriented graphite (~0.335 nm).[22,23] The other two samples, GN and CNT/GN, are found to have the interlayer distances of 0.390 and 0.342 nm, respectively. This deviation of the lattice structure can be attributed to the GN powders, reduced and exfoliated into a monolayer or few-layer states.[24] The oxidation-induced expansion of graphite structure, originated from the presence of residual oxygen-containing functional groups or other structural defects[25]. It is believed that the oxygen groups of GNs can assist the dispersion of CNTs, forming the three-

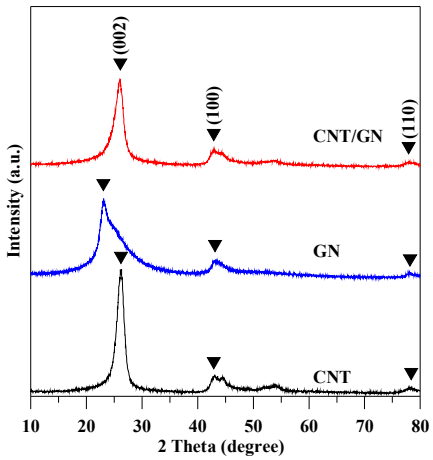

Figure 4. Typical XRD patterns of CNTs, GNs, and CNT/GN composite.

dimensional carbon framework. Accordingly, it is reasonable that the addition of GNs would increase the average interlayer spacing of CNT/GN framework.

The Raman spectra of CNT, GN, and CNT/GN powders are depicted in Figure 5. Herein the Raman band observed at 1580 cm^{-1} can be assigned to a single crystallite of graphite (*G* band), while the other band at 1350 cm^{-1} is attributed to amorphous carbon or deformation vibrations of a hexagonal ring (*D* band).[26-28] The intensity ratio of *D* to *G* bands (I_D/I_G) delivers a clue to identify the graphite degree of carbon-based materials. The I_D/I_G ratios are calculated to be 0.755, 1.066, and 0.873 for the CNT, GN, and CNT/GN samples, respectively. This result reveals that the GN sample shows a poor crystallinity among these carbon materials, originated from the vibration of carbon atoms with dangling bonds in crystal lattice plane terminations of disordered graphite, or from the defects in curved graphene sheets.[29]

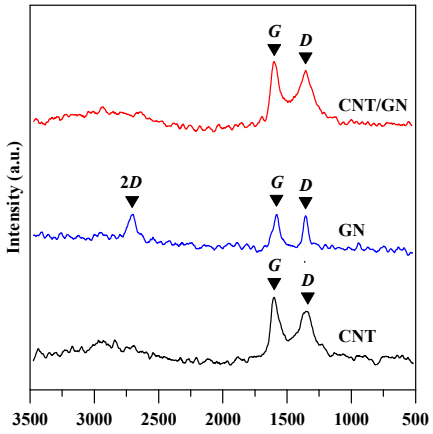

Figure 5. Raman spectra of CNTs, GNs, and CNT/GN composite.

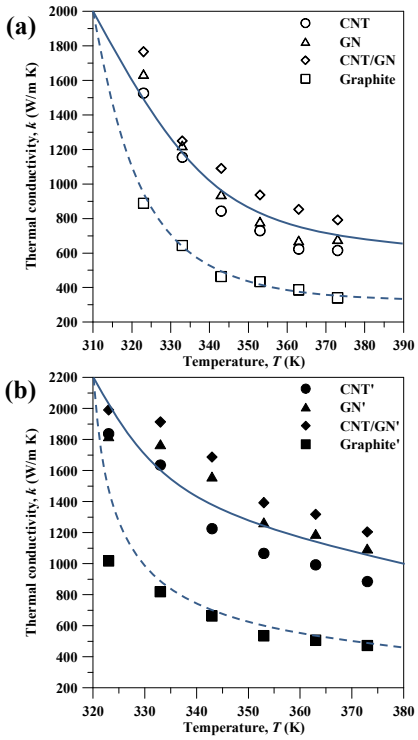

Figure 6. The in-plane thermal conductivity as a function of operating temperature for all heat sinks using CNTs, GNs, and CNT/GN composite: (a) without and (b) with compression process. The thermal conductivity of natural graphite-based heat sink is also given for comparison.

Moreover, the 2*D* band at ~2700 cm^{-1} can be observed in the Raman spectrum of GN sample. It is generally recognized that the position and shape of 2*D* peak are pivotal indicators to distinguish the number of graphene layer. The number of graphene layer falls into the range of 2–5, according to the evolution of standard Raman spectra at 514 nm with the number of layers.[30]

The in-plane thermal conductivity of uncompressed and compressed heat sinks as a function of operating temperature is illustrated in Figure 6a,b, respectively. It can be seen that the k_{ip} values show a decreasing trend with temperature, which is inconsistent with Umklapp phonon-phonon scattering that displays approximately $1/T$ temperature dependence.[1,31]

It is presumably due to one reason that the phonon Umklapp scattering seems to be minor at low temperatures (i.e., the temperature range of 298–373 K in this case). Thus, the thermal property is mainly dominated by phonon-boundary scattering. Data from Figure 6a, the CNT/GN composite exhibits the highest k_{ip} value among these heat sinks, e.g., CNT (1526 W/m K), GN (1637 W/m K), and CNT/GN (1766 W/m K) at 298 K. This variation can be attributed to the lattice vibration and phonon mean free path in different carbon nanostructures. It is well known that the thermal conductivity is proportional to $C_p v l$, where C_p is the heat capacity per unit of volume, v is the speed of sound, and l is

the phonon mean free path.[2,8] The latter quantity strongly depends on scattering from carbon boundaries (i.e., grain size), point defects, and Umklapp processes. The phonon mean free path on single graphene layer (i.e., basal-plane diffusivity) is more diffusive than that on individual CNT. The CNT-based heat sink consists of highly resistive thermal junctions between nanotubes,[14] thereby reducing the thermal transport capability. The schematic diagram for describing three types of thermal transport can be illustrated in Figure 7. The CNT forest provides one-dimensional sp^2 thermal pathway; however, the effective k value of CNTs largely depends on the fraction of nanotubes offering axial conduction paths.[32] The CNT-based heat sink is mainly composed of anisotropic stacking layers, in which a number of thermal junctions appear due to point and line contact. On the other hand, the GN-based heat sink possesses more basal-plane thermal pathways, less thermal junctions, and longer phonon mean free path, inducing a higher k_{ip} value. The improved thermal releasing performance can be attributed to the introduction of GNs with high intrinsic thermal conductivity, originated from the fact that the thermal conductivity of 2D nanostructures is primarily a function of large phonon mean free path across the strong sp^2 bonds in the networks of carbon atoms.[33] The stacking of graphene layers can be considered as continuum, providing more conductive paths for the heat dissipation. For comparison, the in-plane and through-plane thermal conductivities of natural graphite are also given, as shown in Figures 6 and 9. The GN powders used in the present work are chemically exfoliated from the natural graphite, using the modified Hummers' method. The figures reveal two crucial points: (i) both k_{ip} and k_{tp} values of graphite film show a decreasing trend with operating temperature, and (ii) the bulk graphite layer is not beneficial for heat transport, as compared to GN one. This reduced thermal conductivity of graphite-based heat sink is ascribed to the fact that the irregular stacking of graphite powders resembles "disordered arrangement of books", imparting a large number of grain boundaries.

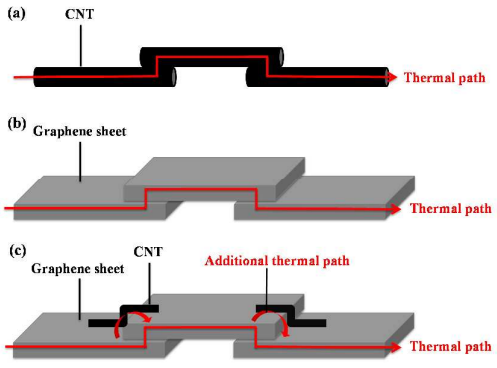

Figure 7. The schematic diagrams for describing different situations of thermal paths in the heat sinks using (a) CNTs, (b) GNs, and (c) CNT/GN composite, showing the interfacial thermal contacts for CNTs (point and line), GNs (edge and plane), CNT/GN (point, line, edge, and plane).

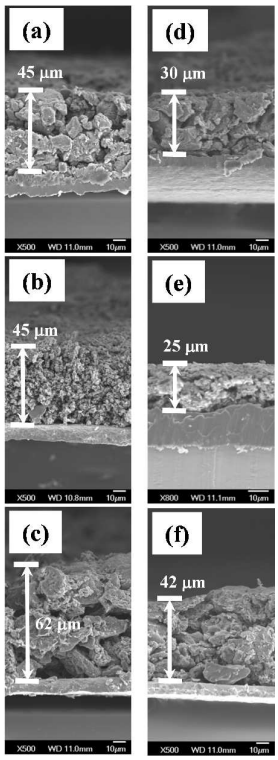

Figure 8. Cross-sectional view FE-SEM photographs for heat sinks without compression ((a) CNTs, (b) GNs, and (c) CNT/GN) and with compression process ((d) CNT', (e) GN', and (f) CNT/GN').

This appearance of boundaries tends to hinder thermal contact, causing a discontinuous thermal transport pathway. Since the size of graphite powder is in microscale, the extent of discontinuous thermal contact becomes more evident. In contrast, the GN layers can serve as smooth silks, covering each other through a preferred orientation. Thus, the GN-based heat sink offers more thermal contact edges and planes, leading to a well-developed thermal transport network. As for the CNT/GN sample, the hierarchical heat sink creates a three-dimensional thermal conductive network that combines with point, line, and plane contact, thus, allowing more efficient heat transport.

As compared with uncompressed heat sinks, there are almost 11–20% improvement of the k_{ip} values for compressed ones, as shown in Figure 6a,b. The k_{ip} value of CNT/GN' heat sink can reach as high as 1991 W/m K. The cross-sectional FE-SEM images of CNT', GN', and CNT/GN' samples are preseted to compare the average thickness of heat sinks before and after the compression process, as depicted in Figure 8. The compression process significantly reduces the thickness of heat sinks with the compression ratio ranging from 22 to 44%. This result reveals that the hierarchical carbon structures become denser than original ones, imparting more thermal conductive area and less thermal resistivity, i.e., a reduced possibility of phonon-boundary scattering.

Therefore, the heat sinks gain a continuous phase (i.e., more thermal pathways), which interconnects the CNTs and GNs in the bulky layer. Accordingly, the compressed heat sinks using carbon nanomaterials (i.e., CNT, GN, and CNT/GN composite) is capable of inducing better thermal conduction. Figure 9a,b illustrate the variation of through-plane thermal conductivity of uncompressed and compressed heat sinks with operating temperature. It can be seen that the k_{tp} value is also a decreasing function of temperature. As expected, a tendency of reduction in k_{tp} with the increase in temperature is observed in all the heat sinks.

In comparison, the magnitude of k_{tp} values is 25–35 times less than that of k_{ip} values. The reduction of k_{tp} values is ascribed to the fact that the thermal conduction of graphite-like materials is strongly limited by phonon transport along the basal plane. It is worth noting that the k_{tp} values at 323 K have two sequences as CNT/GN (57 W/m K) > GN (49 W/m K) > CNT (48 W/m K) and CNT/GN' (76 W/m K) > GN' (58 W/m K) > CNT' (55 W/m K). This result reflects that the CNT/GN' sample delivers the highest through-plane thermal conductivity among the heat sinks. This improved k_{tp} value originates from one reason that the CNT/GN framework offers a stereo stacking architecture, imparting more thermal paths along the vertical direction.

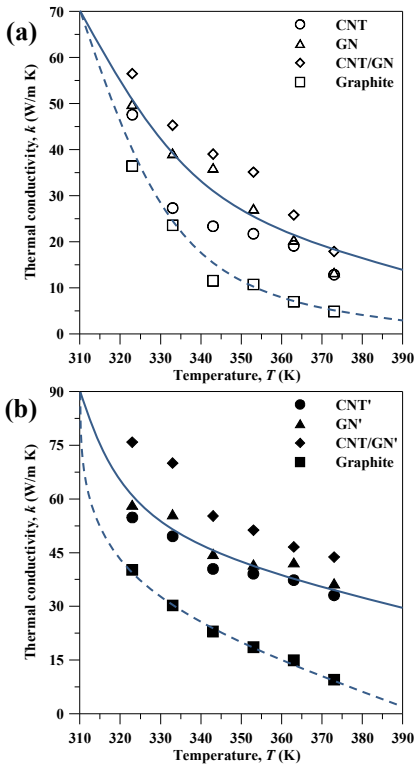

Figure 9. The through-plane thermal conductivity as a function of operating temperature for all heat sinks using CNTs, GNs, and CNT/GN composite: (a) without and (b) with compression process. The thermal conductivity of natural graphite-based heat sink is also given for comparison.

In addition, the compression treatment not only promotes more conjunctions to both ends of CNTs and edges of GNs but also reduces volume content of carbon layers. Such better in-depth and compact connection is the major reason why the CNT/GN' heat sink possesses the highest k_{tp} value. It has been confirmed that thermal conduction in carbon is governed by lattice vibration and phonon transport, in contrast to electrical conduction which is due to free electrons in conductors.[15,34] To figure out the effect of electrical resistivity on thermal property, the relationship between thermal resistivity and electrical resistivity at ambient temperature for graphitized carbons has been examined by Mason and Knibbs in 1962.[35] Unfortunately, the obtained correlation was restricted within the k vale < 400 W/m K and electrical conductivity (ε) < 0.4 × 10^6 S/m. The graphitized carbons selected in that study were mainly extruded artificial graphite materials with an average crystallite size along the basal plane > 20 nm. Figure 10a shows the Mason and Knibbs' correlation between the k and the ε values, in which the k value was extrapolated to approximately 1000 W/m K. For comparison, the relationship between the k_{ip} and the ε values for all heat sinks are also plotted in this figure.

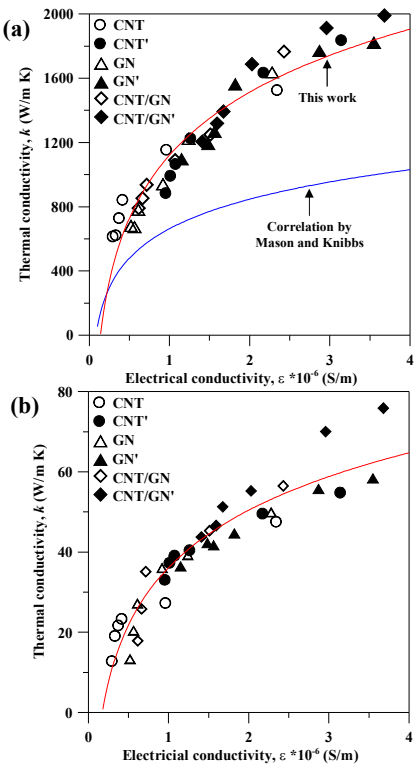

Figure 10. The relationship between thermal conductivity and electrical conductivity of carbon-based heat sinks: (a) in-plane and (b) through-plane thermal conductivities. The correlation made by Mason and Knibbs is given for comparison, in which the thermal conductivity was extrapolated to approximately 1000 W/m K.

It is evident that there is an obvious difference between the correlation by Mason and Knibbs and the correlation obtained from this work. This happens probably because the graphitized materials used by Mason and Knibbs exhibits relatively weak axial orientations and isotropic texture, whereas the present work studied the nanoscaled graphitized materials with one-, two-, and three-dimensional carbon networks. The plot of k_{tp} versus ε value is illustrated in Figure 10b, also showing an increasing trend in the entire region. To describe the relations, two empirical equations are formulated as $k_{ip} = 567 \ln(\varepsilon) + 1120$ and $k_{tp} = 20.6 \ln(\varepsilon) + 36.1$ for in-plane and through-plane thermal conduction, respectively. Herein both the k_{ip} and k_{tp} values are in the units of W/m K and ε is in 10^6 S/m. Through the systematic deduction, the empirical equations with high correlation deliver excellent description concerning the relationship of thermal and electrical conduction. The experimental results are obtained over the 323–373 K range, suitably complementing the thermal management of chips for computer, communication, and consumer electronics. This finding is capable of offering an efficient way to predict the thermal conduction efficiency and heat dissipation performance of heat sinks, based on the nanoscaled graphitized materials. Since the carbon nanomaterials possess low thermal expansion and stable chemical stability, the carbon-based heat sinks can be considered as a potential candidate for wide-range applications of thermal management, e.g., electronic and nano-mechanical devices.

Conclusions

We have presented thermal conductivities from hierarchical heat sinks using CNTs and GNs within the entire temperature region of 323–373 K. A homogenizing method was adopted to prepare three-dimensional CNT/GN framework, offering the higher k value as compared with CNTs and GNs. The k_{ip} and k_{tp} values of CNT/GN-based heat sink could attain as high as 1991 and 76 W/m K at 323 K, respectively. This enhanced thermal conductivity could be attributed to the fact that the hierarchical heat sink provides a three-dimensional thermal conductive network combining with point, line, and plane contact, leading to an efficient heat transport. Moreover, the compression treatment provided an efficient route to increase both k_{ip} and k_{tp} values. This probably originated from the formation of more conjunctions at both ends of CNTs and edges of GNs and reduced volume content of carbon layers. The relationship between k and ε values was well described by two empirical equations: $k_{ip} = 567 \ln(\varepsilon) + 1120$ and $k_{tp} = 20.6 \ln(\varepsilon) + 36.1$ for in-plane and through-plane thermal conduction, respectively. The experimental results were acquired within the 323–373 K range, suitably complementing the thermal management of chips for consumer electronics.

Acknowledgements

The authors are very grateful for the financial support from the Ministry of Science and Techonology (Taiwan) under the contract NSC 101-2628-E-155-001-MY3 and MOST 103-2221-E-155-014-MY2.

References

1. E. Pop, D. Mann, Q. Wang, K. Goodson and H. Dai, Nano Lett., 2006, 6, 96─100.
2. S. Berber, Y. K. Kwon and D. Tomanek, Phys. Rev. Lett., 2000, 84, 20.
3. S. Iijima, Nature, 1991, 354, 56–58.
4. J. Hone, M. Whitney, C. Piskoti and A. Zettl, Phys. Rev. B, 1999, 59, 4.
5. K. S. Novoselov, A. K. Geim, S. V. Morozov, D. Jiang, Y. Zhang, S. V. Dubonos, I. V. Grigorieva and A. A. Firsov, Science, 2004, 306, 666–669.
6. J. Zhang and X. Wang, Nanoscale, 2013, 5, 734.
7. A. A. Balandin, S. Ghosh, W. Bao, I. Calizo, D. Teweldebrhan, F. Miao and C. N. Lau, Nano Lett., 2008, 8, 902–907.
8. H. Tang, G. J. Ehlert, Y. Lin and H. A. Sodano, Nano Lett., 2012, 12, 84–90.
9. L. Xu, N. Wei, Y. Zheng, Z. Fan, H. Q. Wang and J. C. Zheng, J. Mater. Chem., 2012, 22, 1435.
10. J. C. Bokros, Chemistry and physics of carbon, vol. 5, 1969, pp 1─118.
11. S. Zhou, S. Chiang, J. Xu, H. Du, B. Li, C. Xu and F. Kang, Carbon, 2012, 50, 5052–5061.
12. G. Yuan, X. Li, Z. Dong, A. Westwood, Z. Cui, Y. Cong, H. Du and F. Kang, Carbon, 2012, 50, 175–182.
13. Z. Liu, Q. Guo, J. Shi, G. Zhai and L. Liu, Carbon, 2008, 46, 414–421.
14. Q. Wang, X. H. Han, A. Sommers, Y. Park, C. T. Joen and A.Jacobi, International J. Refrigeration, 2012, 35, 7–26.
15. M. Zhou, H. Bi, T. Lin, X. Lü, D. Wan, F. Huang and J. Lin, Carbon, 2014, 75, 314–321.
16. Z. Yan, W. Yao, L. Hu, D. Liu, C. Wang and C. S. Lee, Nanoscale, 2015, 7, 5563.
17. C. T. Hsieh and W. Y. Chen, Carbon, 2010, 48, 612–619.
18. C. T. Hsieh, S. M. Hsu, J. Y. Lin and H. Teng, J. Phys. Chem. C, 2011, 115, 12367–12374.
19. Jr. W. S. Hummers, J. Am. Chem. Soc., 1958, 80, 1339.
20. S. Zhou, J. Xu, Q. H. Yang, S. Chiang, B. Li, H. Du, C. Xu and F. Kang, Carbon, 2013, 57, 452–459.
21. C. T. Hsieh, Y. Y. Liu, D. Y. Tzou and W. Y. Chen, J. Phys. Chem. C, 2009, 116, 26735–26743.
22. R. Sengupta, M. Bhattacharya, S. Bandyopadhyay and A. K. Bhowmick, Prog. Polym. Sci., 2011, 36, 638–670.
23. Q. M. Gong, Z. Li, Y. Wang, B. Wu, Z. Zhang and J. Liang, Mater. Res. Bull., 2007, 42, 474.
24. S. Wang, Y. Zhang, N. Abidi and L. Cabrales, Langmuir, 2009, 25, 11078.
25. C. Wang, D. Li, C. O. Too, and G. G. Wallace, Chem. Mater., 2009, 21, 2604.

26. Y. T. Lee, N. S. Kim, J. Park, J. B. Han, Y. S. Choi, H. Ryu and H. J. Lee, Chem. Phys. Lett., 2003, 372, 853–859.
27. K. E. Kim, K. J. Kim, W. S. Jung, S. Y. Bae, J. Park, J. Choi and J. Choo, Chem. Phys. Lett., 2005, 401, 459–464.
28. L. Ni, K. Kuroda, L. P. Zhou, T. Kizuka, K. Ohta, K. Matsuishi and J. Nakamura, Carbon, 2006, 44, 2265–2272.
29. C. W. Huang, C. H. Hsu, P. L. Kuo, C. T. Hsieh and H. Teng, Carbon, 2011, 49, 895–903.
30. A. C. Ferrari, J. C. Meyer, V. Scardaci, C. Casiraghi, M. Lazzeri and F. Mauri, Phys. Rev. Lett., 2006, 97, 187401–187404.
31. J. M. Ziman, Oxford University Press: Oxford, 2001.
32. N. K. Mahanta, A. R. Abramson, M. L. Lake, D. J. Burton, J. C. Chang, H. K. Mayer and J. L. Ravine, Carbon, 2010, 48, 4457–4465.
33. R. J. Warzoha, D. Zhang, G. Feng and A. S. Fleischer, Carbon, 2013, 61, 441–457.
34. P. Keblinski, S. Phillopt, S. Choi and J. Eastman, Int. J. Heat Mass Transfer, 2002, 45, 855–863.
35. I. B. Mason and R. H. Kinbbs, United Kingdom Atomic Energy Authority, 1962, AERE-R 3973.